Correlation and Spectral Analysis of Distance-Dependent DGPS Errors Over a Regional Network

G. Fotopoulos and C. Kotsakis
Department of Geomatics Engineering, University of Calgary
2500 University Drive N.W., Calgary, Alberta, Canada, T2N 1N4, Email: gfotopou@ucalgary.ca

Abstract

The purpose of this paper is to investigate the spatial and temporal behaviour of various error sources affecting precise DGPS positioning, using covariance and spectral analysis techniques on data collected over a network of permanent GPS reference stations. Such permanent network arrays are employed for a variety of precise positioning applications, including tectonic deformation monitoring, post-glacial rebound studies and many other geodynamic applications. Combined corrections containing ionospheric, tropospheric and satellite orbit effects are estimated from measurements gathered over a network of GPS reference stations spanning approximately a 400 km by 300 km area in southern Sweden. Different gridding techniques are used to parameterize these corrections over the network coverage area. By computing the correlation and power spectral density functions of the gridded corrections, which are generated at various grid resolutions, valuable insight into the frequency content and behaviour of the DGPS data errors is obtained.

1 Introduction – GPS Multiple Reference Station Approach

The use of several reference stations in a wide area differential GPS (WADGPS) network to improve the accuracy of code-based GPS positioning has been employed with great success, both in post-processing and real-time modes (Kee and Parkinson, 1992). A natural extension of this concept is to use the more precise carrier phase GPS measurements in a similar network approach. However, the transition from code-based to carrier phase-based schemes is not a trivial task, mainly due to the more stringent accuracy requirements in the latter case, which expose new and challenging problems. For instance, in most code-based DGPS positioning approaches the limiting error sources are mainly the measurement noise and multipath of the code itself (ionospheric effects come into play only over longer baseline distances, i.e. several tens of kilometres). Other error sources such as atmospheric and satellite orbit, the effects of which were somewhat masked by the low accuracy requirements in code-based DGPS, are brought to the forefront in carrier phase-based techniques. Also, the precise and reliable resolution of integer ambiguities is very critical for high accuracy carrier phase-based positioning. Finally, the need to meet competitive requirements for real-time users uncovers many important issues related to the optimal parameterization of measurement error corrections and their dissemination/communication to potential GPS users located within (or surrounding) the reference network coverage area (Fotopoulos, 2000).

Recently, the use of multiple reference stations, instead of standard single baseline carrier phase approaches, has been receiving a significant amount of attention from the GPS community. This is mainly due to the fact that the implementation of multiple reference stations in a permanent array for performing carrier phase-based DGPS positioning offers several advantages over the standard single baseline approach. Some of the advantages for multi-reference station network users, as compared to single baseline users, are:

- increase in reliability and availability of service,
- modelling of the distance-dependent or spatially correlated error sources,
- improvement in ambiguity resolution over longer baselines,
- larger coverage area in DGPS positioning applications, and
- generation of observations for a *fictitious* or virtual reference station (VRS).

There are also certain drawbacks associated with using a network of GPS reference stations, such as an increase in data transmission load, an increase in complexity of user implementation, and an inevitable increase in costs for network operators and providers. In general, however, the advantages provided by the permanent array approach, combined with the multitude of effort that has been placed on formulating algorithms and processing methodologies, take precedence in providing GPS users with an efficient and reliable multi-reference station carrier phase-based solution.

1.1 Correction Generation Algorithm

Several methods for formulating corrections to GPS observations from reference station data have been developed over the past few years, such as the partial derivative algorithms (as per Wübbena et al., 1996), linear interpolation algorithms (as per Wanninger, 1997), and the conditional adjustment algorithm (as per Raquet, 1998). An overview of these methods is given in Fotopoulos and Cannon (2000).

The algorithm selected for computing the GPS corrections that were used in the spectral investigations presented in this paper is the conditional adjustment algorithm (CAA), developed by Raquet (1998) at the University of Calgary. This approach predicts correction values for the carrier phase measurements based on the estimated behaviour of the distance-dependent errors, over a network of reference stations. Essentially, a conditional least-squares adjustment is applied to the reference network data such that the double differences of the adjusted measurements minus the calculated ranges are zero, which is valid in the absence of any errors. More details on the derivation and application of this method can be found in Raquet (1998). For the purposes of the analysis that follows, it is important to understand that the corrections are generated for each visible satellite over the network stations, on a satellite-by-satellite basis (referred to as satellite-based corrections) every epoch. A prerequisite to implementing the CAA is the provision of accurate reference station coordinates, which may be provided by the responsible authority in the case of a permanent regional reference network, or they may be obtained through a static survey of each station over long periods. In addition, the correct double difference integer ambiguities between the reference stations must be known.

1.2 Test Network

The Swedish Permanent GPS Network, commonly referred to as the SWEPOS network, is a national network of 21 permanent reference stations which span all of Sweden with an average separation of 200 km. The network was established in August of 1993 by the National Land Survey of Sweden and the Onsala Space Observatory. Each station is equipped with two Ashtech Z-XII dual frequency receivers and a Dorne-Margolin antenna; for more details, see Hedling and Jonsson (1996). The network is used for various applications requiring metre to millimetre levels of accuracy.

A 24-hour continuous data set that was collected on September 16, 1998 at 1 Hz is used for the results presented herein. A smaller subnetwork consisting of eight of the southern SWEPOS stations (SSN) was chosen for our analysis, see Fig. 1. In general, the data was of high quality with few cycle slips identified. The SSN covers approximately a 373 km × 262 km area. All processing was performed on an epoch-by-epoch basis, simulating real-time, with the exception of the resolution of the double difference ambiguities which were computed a-priori using GPSurvey™ (Trimble Navigation Limited).

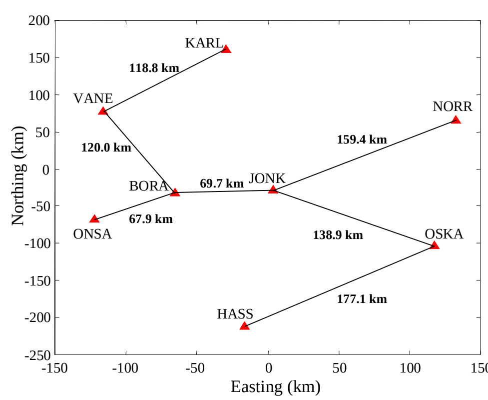

Fig. 1 Test network and independent baseline solutions

2 Grid-Based Parameterization

A number of schemes can be implemented for parameterizing the corrections generated for the network coverage area, such as a best-fit plane (Wübbena et al., 1996), low-order surface models, and grid-based interpolation schemes (Fotopoulos, 2000). Regardless of the parameterization method, the main objective is always the approximation of a surface that represents the spatial variation of the data errors, thus providing a solid foundation of the correction field behaviour over the area of interest. In our case, a grid-based parameterization scheme was used, which involved the computation of combined corrections at gridded locations over the reference network area and then interpolation between grid nodes for any user located within or surrounding the coverage area.

The gridded corrections were generated using the CAA for each satellite visible over the SSN during the 24-hour data period. The horizontal grid point locations vary, depending on the grid resolution and the limits of the reference station network. A sample of a satellite-based correction field generated for the distance-dependent errors at 14:00 hours local time, over the SSN, is shown in Fig. 2.

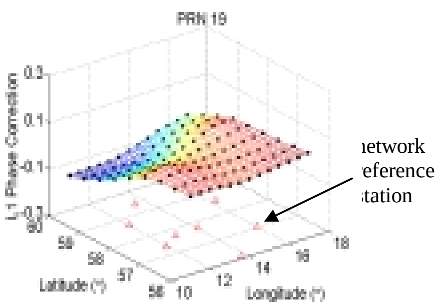

Fig. 2 Correction field for distance-dependent errors (in cycles)

3 Temporal Correlation Analysis

One of the key concerns for providers and users of regional GPS networks is the provision of timely corrections which adhere to transmission bandwidth limitations. A useful tool for studying the variation of the correction values over time is to compute the discrete autocorrelation function corresponding to the satellite-based correction field, as follows:

$$R(kT) = \sum_{n=0}^{N-1} g[nT]\, g[(n+k)T] \tag{1}$$

where $g[nT]$ represents a sampled time series of corrections corresponding to a specific satellite and evaluated by interpolating between grid nodes for an arbitrary user location. In our case, a point near the centre of the SSN (Fig. 1) was chosen for the user location. The duration of the correction time series depended on the visibility of the satellite over the network (averaging three to four hours in most cases). To compute the autocorrelation functions of the distance-dependent errors over time, representative samples of correction time series were first evaluated. The corrections were generated on a per satellite basis for two main periods during the 24-hour data set, (a) 12:00 am to 4:00 am and (b) 11:00 am to 3:00 pm, which respresent the 'quiet' and 'active' periods respectively, according to the expected relative ionospheric activity. In addition, the autocorrelation functions were computed during these periods, for both combined L1 phase and ionospheric-free (IF) corrections (see Raquet, 1998) as shown in Fig. 3. To allow for consistent comparisons, all corrections were estimated for a user located near the centre of the network in both cases (a) and (b) described above.

The results of the autocorrelation functions varied between satellites. However, some general observations can be made about the representative samples investigated. Some of the autocorrelation functions showed a strong correlation over a larger time, indicating a smoother signal that is easier to model. In a few cases the autocorrelation functions closely resemble an exponential trend, as evidenced in Figure 3. Here, the functions decrease strongly for small time differences. This indicates a rougher signal with higher frequency variations, which are generally more difficult to model than smoother, slowly changing behaviour.

Of interest for our analysis are the values of two basic parameters of the autocorrelation functions, namely the mean square value (maximum value at the origin) and the correlation length (time lag corresponding to the point where the function takes on half of the mean square value). Long correlation lengths indicate a much smoother, more easily modelled signal. The correlation lengths for two of the satellite correction series investigated are indicated by arrows in Fig. 3. The corresponding mean square values, associated with the combined and ionospheric-free correlation functions, during the 'quiet' period, show that the IF values are greater in most cases. This means that the ionospheric-free signal is stronger than the combined L1 signal. A possible explanation for this is the randomness of the effects of the residual errors observed thus far, which may cancel to some degree when combined to form one correction. Also the decorrelating behaviour of the most dominant effect in the combined corrections, namely the ionosphere, may be responsible for reducing the strength of the signal according to its` activity. The correlation lengths associated with the set of satellites investigated during the 'quiet' period ranged from 840 s to 1860 s for the combined corrections, and 150 s to 3375 s for the IF case.

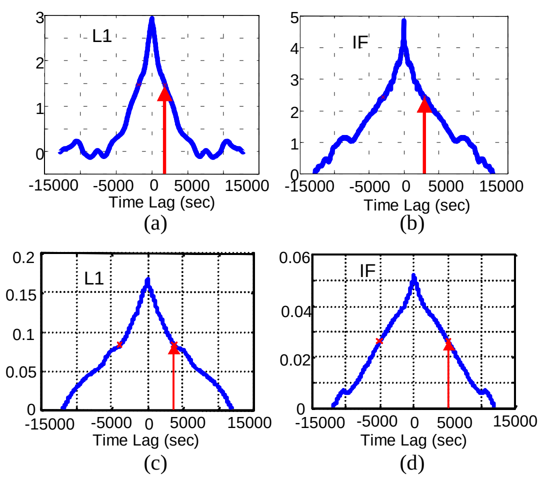

Fig. 3 Sample Autocorrelation Functions for 'Quiet' Period (a and b in units $\times 10^{-3}$ cm^2) and 'Active' Period (c and d in units cm^2)

Investigations conducted for the 'active' period (11:00 am to 3:00 pm) provide a better indication of the behaviour of the corrections because of the more amplified effects of the ionosphere. During this second period, the mean square values for the combined L1 signal are greater (for the majority of the samples) than the corresponding ionospheric-free corrections. The more active ionosphere is the cause of this behaviour (see Figs. 3c and 3d). A possible explanation for the satellite correction series where the IF signal is stronger than the L1 is the presence of residual or 'unmodelled' ionospheric effects. Thus, it is likely that unmodelled systematic behaviour is the cause of these strong autocorrelation functions. However, in general the results support the fact that the combined signal is much stronger than the ionospheric-free signal during this period of a relatively active ionosphere. A summary of the autocorrelation function parameters for the two time periods is provided in Table 1 for the combined L1 corrections and the IF values are shown in brackets.

A direct comparison between the two time periods cannot be made, due to the different satellites involved. However, of relevance for the temporal analysis are the overall large correlation lengths on the order of several thousands of seconds, which translates to tens of minutes. This is encouraging as it reflects the relatively slow variability in parameterized corrections computed for the user location. Similar results reflecting these temporal trends were obtained in the position domain analysis of Fotopoulos (2000). It should also be noted that in many cases the autocorrelation function parameters for the same satellites, corresponding to combined (three error sources - L1 phase) and separated (two error sources - IF) signals, were significantly different. These differences support the concept of separating the error sources (at least the ionospheric effects), in order to formulate more consistent information for the user. Further investigations must be conducted on this matter.

Table 1 Autocorrelation Function Parameters for L1 (IF)

SV	MSV (cm2)	Correlation Length (s)
Quiet Period (12:00 am to 4:00 am)		
6	0.0029 (0.0049)	1860 (3045)
10	0.0063 (0.0132)	840 (150)
17	0.0124 (0.0122)	1815 (1365)
22	0.0069 (0.0294)	1560 (3375)
25	0.0134 (0.0197)	1200 (1125)
Active Period (11:00 am to 3:00 pm)		
4	0.0335 (0.0051)	5565 (855)
14	0.1383 (0.1885)	1470 (2985)
16	0.1664 (0.0522)	3765 (5070)
18	0.0131 (0.0523)	2100 (3540)
24	0.2243 (0.0154)	3240 (1080)

4 Spectral Analysis

In this section, the spectral properties of the satellite-based correction fields, as shown in Fig. 2, is investigated by examining their power spectral density (PSD) functions. As opposed to the temporal correlation analysis of the previous section, this analysis involves the gridded correction surfaces computed at a particular epoch in time. Since the spatial dimensionality of the problem has been defined as being two-dimensional with horizontal components in the latitudinal (y) and longitudinal (x) directions, it is necessary to compute the 2D discrete Fourier Transform (DFT), as per Sideris (1984), for the gridded corrections $h(k\Delta x, \ell\Delta y)$:

$$H\left(mf_X, nf_Y\right) = \frac{T_X T_Y}{MN} \sum_{k=0}^{M-1} \sum_{\ell=0}^{N-1} h\left(k\Delta x, \ell \Delta y\right) e^{-j2\pi\left(\frac{mk}{M} + \frac{n\ell}{N}\right)} \tag{2}$$

where Δx, Δy are the grid spacings in the x and y directions respectively, T_X, T_Y are the corresponding spatial periods, and M, N are the number of grid points along the x and y directions respectively. The corresponding 2D PSD is easily derived from the squared magnitude of the DFT, as shown below:

$$P_h = \left| H\left(mf_X, nf_Y\right) \right|^2 \tag{3}$$

The evaluation of the PSD function, through Eq. (3), permits the detection of dominant spatial frequencies contributing to the data. In this case, the data is a set of gridded values containing formulated corrections for the correlated error sources based on a regional network. The corresponding grid spacings, Δx and Δy, vary depending on the resolution of the parameterization scheme (i.e. 0.5°, 1.0°, etc.). This spatial resolution is also related to the extent of the frequencies over which the PSD is defined, as will be observed in the results that follow.

Numerous investigations were conducted on the satellite-based correction fields in order to determine their corresponding spectral properties. Variations in satellite elevation, epoch and parameterization scheme were evaluated. Fig. 4 (left) shows the PSD function resulting from the correction filed of a very high elevation satellite (approximately 85°, also used as the base satellite for the double difference computations at this epoch) visible at 1:00 pm. Here the correction field was computed using the grid-based parameterization scheme with the highest resolution level, namely $\Delta x = \Delta y = 0.5°$. The larger values near the origin of the PSD plot reveal the dominant lower frequencies, which contribute the most to the correction values. These lower frequency components correspond to long wavelength GPS errors, which typically change more slowly and are thus easily modelled. More specifically, the low frequency range along the x-direction is less than 0.2 cycles/degree longitude, whereas along the y-direction it nearly doubles, reaching 0.4 cycles/degree latitude. This indicates relatively higher variations in the north-south component than the east-west. Overall, the PSD functions are concentrated near the origin approaching zero at higher frequencies and appear to be uncontaminated by aliasing effects resulting from poorly sampled data.

Results for the same correction field described above were generated for a sparser grid resolution where $\Delta x = \Delta y = 1.0°$. The computed PSD function is also shown in Fig. 4 (right). Note that the higher spacing affects the recoverable frequency range, limiting its extent to ± 0.5 cycles/degree. Since the majority of the frequency components are contained within this range, it is evident that the low frequency information is still maintained with the sparser grid parameterization. However any higher frequency information beyond ± 0.5 cycles/degree is lost. This aliasing effect is amplified when the grid resolution is further decreased to $\Delta x = \Delta y = 1.5°$. In this case, the corresponding recoverable frequency range is decreased to ± 0.33 cycles/degree, which means that there is a loss of information, especially for the upper limits of the predominant frequencies along the y-direction.

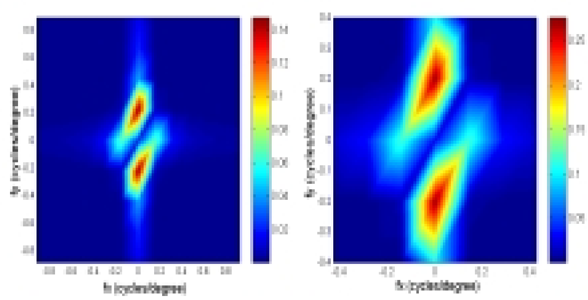

Fig. 4 2D PSD Functions for SV 18, $0.5° \times 0.5°$ (left) and $1° \times 1°$ (right) Grid-Based Parameterization

Additional samples of correction fields visible at the same epoch, but for lower elevation satellites (averaging 25°) were also evaluated. In all cases, significantly larger amplitudes compared to the higher elevation cases were noted. This can be explained from the elevation of the satellite, which is much lower and therefore incurs a higher level of atmospheric activity that is accounted for by higher correction values. The amplitudes associated with the lower frequency components are again dominant, corresponding to longer wavelength trends in the correction field. The dominant lower frequency ranges in these cases varied from ± 0.2 cycles/degree in both horizontal component directions. As opposed to the higher elevation satellite cases, the larger PSD values are concentrated mainly in an east-west direction. Thus, the directional behaviour of the correction field varies depending on the satellite elevation, however further studies must be conducted in order to determine other factors that may contribute to this effect.

The aforementioned examples are useful for identifying the dominant frequency contributions for the entire network coverage area. The relative strength of the signal is magnified according to the selected epoch in time when the correction field is investigated. Since the examples discussed thus far are obviously affected by stronger ionospheric activity, it is useful to examine some cases where the ionospheric activity is relatively lower. To accomplish this, correction fields were generated at high and low elevations for an epoch in the morning hours at approximately 3:00 am. Results for the higher resolution grid-based parameterization depicts essentially the same spectral behaviour associated with the complementing scenario visible during the midday period (1:00 pm). Additional tests were conducted in the same manner for other correction fields, however the plots are not included here as they would be redundant. In all cases, it was found that the majority of the frequency information is retained up to a grid resolution of $\Delta x = \Delta y \leq 1.0^\circ$. Once the resolution is decreased by implementing sparser grid-based parameterizations, some of the dominant low frequency information is distorted and some higher frequency information is lost.

5 Conclusions

The analysis conducted in this paper provided valuable insight into the behaviour of the satellite-based correction fields. From a temporal perspective, large correlation lengths on the order of several tens of minutes indicate slowly changing correction values. This emphasizes the feasibility of updating model parameters over several minutes, which significantly reduces the transmission bandwidth load. Also, differences between the combined L1 phase autocorrelation functions and the ionospheric-free autocorrelation functions were noticed, which introduces the need for modelling each error source separately (to some degree). From a spatial perspective, the spectral analysis of various correction fields showed that grid resolutions of $0.5^\circ \times 0.5^\circ$ and $1^\circ \times 1^\circ$ were adequate for maintaining the frequency information contributing the most to the Swedish network data.

References

Fotopoulos G. and Cannon M.E. (2000) An Overview of Multi-Reference Station Methods for Cm-Level Positioning. *GPS Solutions*, vol. 4, John Wiley & Sons, Inc. (in print)

Fotopoulos G. (2000) Parameterization of DPGS Carrier Phase Errors Over a Regional Network of Reference Stations. *MSc. Thesis*, University of Calgary, Department of Geomatics Engineering, Report No. 20142, Calgary, Alberta.

Hedling G. and Jonsson B. (1996) New Developments in the SWEPOS Network. In *Proceedings of the 9th International Technical Meeting of the Satellite Division of the Institute of Navigation (ION GPS-96)*, Kansas City, Missouri, pp. 1803-1808.

Kee C. and Parkinson B. (1992) Algorithms and Implementation of Wide Area Differential GPS. In *Proceedings of the 5th International Technical Meeting of the Satellite Division of the Institute of Navigation (ION GPS-92)*, Albuquerque, New Mexico, pp. 565-572.

Raquet J. (1998) Development of a Method for Kinematic GPS Carrier-Phase Ambiguity Resolution Using Multiple Reference Receivers. *Ph.D. Thesis*, University of Calgary, Department of Geomatics Engineering Report No. 20116, Calgary, Alberta.

Sideris M.G. (1984) Computation of Gravimetric Terrain Corrections Using Fast Fourier Transform Techniques. *MSc. Thesis*, University of Calgary, Department of Geomatics Engineering, Report No. 20007, Calgary, Alberta.

Wanninger L. (1997) Real-Time Differential GPS Error Modelling in Regional Reference Station Networks. *In Proceedings of the International Association of Geodesy Symposia* (Advances in Positioning and Reference Frames), vol. 118, pp. 86-92.

Wübbena G., Bagge A., Seeber G., Volker B. and Hankemeier P. (1996) Reducing Distance Dependent Errors for Real-Time Precise DGPS Applications by Establishing Reference Station Networks. In *Proceedings of the 9th International Technical Meeting of the Satellite Division of the Institute of Navigation (ION GPS-96)*, Kansas City, Missouri, pp. 1845-1852.